AIP | Applied Physics Letters

Composition-induced structural, electrical, and magnetic phase transitions in AX-type mixed-valence cobalt oxynitride epitaxial thin films

Jumpei Takahashi, Yasushi Hirose, Daichi Oka, Shoichiro Nakao, Chang Yang, Tomoteru Fukumura, Isao Harayama, Daiichiro Sekiba, and Tetsuya Hasegawa

Citation: Applied Physics Letters **107**, 231906 (2015); doi: 10.1063/1.4937431
View online: http://dx.doi.org/10.1063/1.4937431
View Table of Contents: http://scitation.aip.org/content/aip/journal/apl/107/23?ver=pdfcov
Published by the AIP Publishing

Composition-induced structural, electrical, and magnetic phase transitions in *AX*-type mixed-valence cobalt oxynitride epitaxial thin films

Jumpei Takahashi,[1,2] Yasushi Hirose,[1,2,3,a)] Daichi Oka,[1,2] Shoichiro Nakao,[2,3] Chang Yang,[1,2,3] Tomoteru Fukumura,[1,2,3] Isao Harayama,[4] Daiichiro Sekiba,[4] and Tetsuya Hasegawa[1,2,3]

[1]*Department of Chemistry, School of Science, The University of Tokyo, 7-3-1 Hongo, Bunkyo, Tokyo 113-0033, Japan*
[2]*Kanagawa Academy of Science and Technology (KAST), 3-2-1 Sakado, Takatsu, Kawasaki 213-0012, Japan*
[3]*CREST, Japan Science and Technology Agency, 7-3-1 Hongo, Bunkyo, Tokyo 113-0033, Japan*
[4]*University of Tsukuba Tandem Accelerator Complex (UTTAC), 1-1-1 Tennoudai, Tsukuba, Ibaraki 305-8577, Japan*

(Received 23 August 2015; accepted 25 November 2015; published online 10 December 2015)

Synthesis of mid- to late-transition metal oxynitrides is generally difficult by conventional thermal ammonolysis because of thermal instability. In this letter, we synthesized epitaxial thin films of *AX*-type phase-pure cobalt oxynitrides (CoO_xN_y) by using nitrogen-plasma-assisted pulsed laser deposition and investigated their structural, electrical, and magnetic properties. The CoO_xN_y thin films with $0 \leq y/(x+y) \leq 0.63$ grown on MgO (100) substrates showed a structural phase transition from rock salt (RS) to zinc blend at the nitrogen content $y/(x+y) \sim 0.5$. As the nitrogen content increased, the room-temperature electrical resistivity of the CoO_xN_y thin films monotonically decreased from the order of $10^5\,\Omega\,cm$ to $10^{-4}\,\Omega\,cm$. Furthermore, we observed an insulator-to-metal transition at $y/(x+y) \sim 0.34$ in the RS-CoO_xN_y phase, which has not yet been reported in Co^{2+}/Co^{3+} mixed-valence cobalt oxides with octahedral coordination. The low resistivity in the RS-CoO_xN_y phase, on the $10^{-3}\,\Omega\,cm$ order, may have originated from the intermediate spin state of Co^{3+} stabilized by the lowered crystal field symmetry of the $CoO_{6-n}N_n$ octahedra ($n = 1, 2, \ldots 5$). Magnetization measurements suggested that a magnetic phase transition occurred in the RS-CoO_xN_y films during the insulator-to-metal transition. These results demonstrate that low-temperature epitaxial growth is a promising approach for exploring novel electronic functionalities in oxynitrides. © *2015 AIP Publishing LLC*. [http://dx.doi.org/10.1063/1.4937431]

In the last decade, early transition metal oxynitrides have attracted much attention as nontoxic inorganic pigments[1–3] and visible-light active photocatalysts[3–6] because they have good chemical stability and their band structure is suitable for visible light response. These early transition metal oxynitrides are widely synthesized by thermal ammonolysis, where precursor oxides are partially nitrided under high-temperature ammonia flow. In contrast, mid- to late-transition metal oxynitrides have been scarcely studied till date.[7,8] This is the case mainly because it is difficult to synthesize these materials by thermal ammonolysis: high-temperature ammonia reduces the precursor oxides of mid- to late-transition metals to their corresponding metals.[9] Indeed, among the ternary oxynitrides of 3*d*-transition metals, only TiO_xN_y,[10] VO_xN_y,[11] and CrO_xN_y[12] have been synthesized by thermal ammonolysis.

Highly non-equilibrium, thin film growth techniques such as physical and chemical vapor deposition are promising methods for synthesizing oxynitrides of mid- to late-transition metals such as Fe[13] and Co.[14] For example, Crawford *et al.* used chemical vapor deposition with a $Co(CO)_3NO$ source to synthesize zinc blende (ZB) $CoO_{0.5}N_{0.5}$ thin films, which exhibited a low electrical resistivity of $\sim 10^{-3}\,\Omega\,cm$ at room temperature.[14] The fact that such low resistivity has not been achieved in cobalt oxides with Co^{2+}/Co^{3+} mixed valence[15–18] suggests that unusual electronic states might be realized in oxynitrides. However, the electrical properties of the films have not been investigated in detail, partly owing to insufficient sample quality: the reported $CoO_{0.5}N_{0.5}$ films were polycrystalline with incompletely reacted amorphous phases as impurities.[14] Furthermore, the crystal structure and physical properties of CoO_xN_y have not been reported, except for those of $CoO_{0.5}N_{0.5}$. Because the end members of *AX*-type CoO_xN_y have totally different electronic properties and crystal structures—CoO is an antiferromagnetic insulator with rock salt (RS) structure ($a = 4.263$ Å),[19] and CoN is a paramagnetic metal with ZB structure ($a = 4.28$ Å)[20]—varying the anion composition would induce structural, electrical, and/or magnetic phase transitions. Thus, in the present study, we synthesized epitaxial thin films of phase-pure *AX*-type CoO_xN_y with systematically controlled anion composition and investigated their crystal structures and physical properties.

CoO_xN_y thin films were fabricated on single-crystalline substrates of MgO (100) ($a = 4.213$ Å) and $MgAl_2O_4$ (MAO) (111) ($a/2 = 4.042$ Å) by nitrogen-plasma-assisted pulsed laser deposition (NPA-PLD). The details of NPA-PLD are described elsewhere.[21–23] In brief, a CoO pellet (99.9% purity), sintered in an Ar atmosphere at 1000 °C for 12 h, was ablated by a KrF excimer laser ($\lambda = 248$ nm, $0.66\,J\,cm^{-2}\,pulse^{-1}$). The substrate temperature (T_s) during growth was varied from 160 to 250 °C by an infrared lamp heater. The distance between the ablation target and the substrate was set at 50 mm. N_2 gas activated by

a)Author to whom correspondence should be addressed. Electronic mail: hirose@chem.s.u-tokyo.ac.jp

a radio-frequency (RF) plasma source (SVT Associates, model 4.5 in.) was introduced into the growth chamber as process gas. The input power of the RF plasma source was fixed at 200 W. The nitrogen content of each film was controlled by the partial pressure of nitrogen (P_{N_2}) and the deposition rate (r), which differed as a function of the pulse repetition rate of the excimer laser (1, 2, and 4 Hz). The deposition rate was determined from the deposition time and the film thickness evaluated by using a stylus profiler (Veeco, Dektak 6M). The thicknesses of the films were ~50–105 nm.

The crystal structures of the obtained films were determined by X-ray diffraction (XRD) with a four-axis diffractometer (Bruker AXS, d8 discover) using Cu Kα radiation. The chemical compositions of the films were evaluated by scanning electron microscopy coupled with energy dispersive X-ray spectroscopy (SEM-EDX) (JEOL, JSM-7100F with JED-2300). The SEM-EDX results were calibrated to a standard curve made from performing heavy ion elastic recoil detection analysis (ERDA) on several CoO_xN_y thin films. ERDA measurements were performed with a 38.4 MeV ^{35}Cl beam generated by a 5 MV tandem accelerator (Micro Analysis Laboratory, Tandem Accelerator, The University of Tokyo [MALT]). The recoils of nitrogen were identified by a ΔE–E telescope detector, comprising a gas ionization chamber and a Si solid-state detector. The experimental errors in x and y are about ±10%. The electrical resistivity was determined by using the four-probe method (Quantum Design, PPMS Model 6000) with Ag electrodes deposited by sputtering, of which ohmic contact was confirmed by current-voltage measurements. The magnetic properties were investigated by using a superconducting quantum interference device magnetometer (Quantum Design, MPMS-XL), applying the magnetic field perpendicular to the film surface. The absence of ferromagnetic impurities, such as metallic Co or Co_4N, was confirmed by measuring the magneto-optical Kerr effect at room temperature.

To obtain epitaxial thin films of CoO_xN_y, the T_s was first optimized at fixed r (~15 nm/h) and P_{N_2} (1×10^{-5} Torr). As shown in Fig. 1, CoO_xN_y thin films with pseudocubic structure (RS or ZB, discussed later) grew epitaxially on both MgO (100) and MAO (111) at T_s of 160–250 °C. However, at $T_s = 250$ °C, the sample on the MAO (111) substrate had a secondary phase of Co metal, which probably originated from thermal decomposition of CoO_xN_y, or (111)-oriented CoO_xN_y. In addition, the peak intensity weakened at higher temperatures on the MgO (100) substrate (Fig. 1(a), inset). Thus, in further experiments, we grew CoO_xN_y thin films on MgO (100) at $T_s = 160$ °C.

Figure 2(a) plots the nitrogen contents $y/(x+y)$ of the CoO_xN_y thin films as functions of r and P_{N_2}. With increasing r, i.e., with increasing the relative supply rate of Co and O under the same P_{N_2}, the nitrogen content monotonically deceased, whereas it increased with increasing P_{N_2}. By tuning these two parameters, the anion composition of the CoO_xN_y thin film could be controlled within the range of $0 \le y/(x+y) \le 0.63$. While the O/Co ratio x systematically decreased with increase of nitrogen amount $y/(x+y)$, the (N + O)/Co ratio $x+y$ were almost constant at unity (Fig. 2(b)), indicating the formation of AX-type compounds.

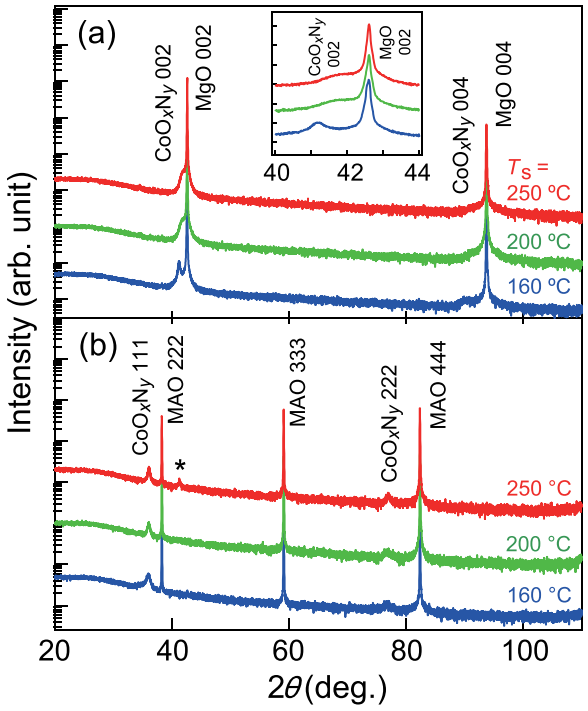

FIG. 1. θ–2θ XRD patterns of CoO_xN_y thin films grown at various T_s on (a) MgO (100) and (b) MAO (111) substrates. The inset in (a) shows magnified plots near the 002 diffraction peaks. The asterisk in (b) indicates the diffraction peak of Co (111) or RS-CoO_xN_y (002) from secondary phase.

Next, we discuss the crystal structures of the CoO_xN_y thin films in detail. The θ–2θ XRD patterns (Fig. 3) and φ scans (see supplementary Fig. S1[24]) of the films with various nitrogen contents revealed that all the films grew epitaxially on the substrate in a cube-on-cube manner without forming any impurity phases. The absence of Pendellosung fringe (Fig. 3(b)) is plausibly due to surface roughness of the films (several nanometers). As possible crystal structures with a pseudocubic cell, we considered A_3X_4-type spinel as well as AX-type RS and ZB structures. Among these three candidates, we excluded A_3X_4-type spinel from the asymmetric scan of hhh diffraction because none of the films showed the 111 diffraction characteristic of the spinel structure ($2\theta \sim 18°$). This result was consistent with the composition analysis (Fig. 2(b)). The intensity ratio of 111 to 002

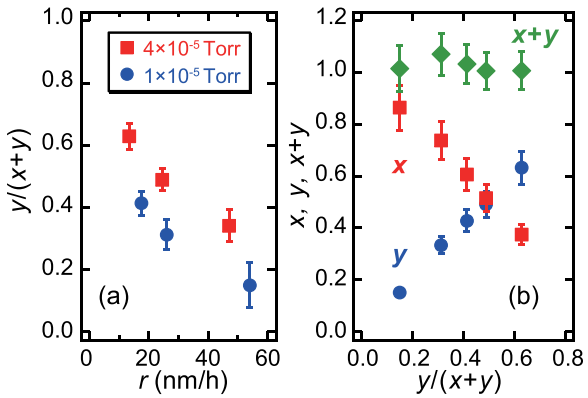

FIG. 2. (a) Nitrogen contents $y/(x+y)$ of the CoO_xN_y thin films grown on MgO (100) with varying deposition rate and nitrogen partial pressure. (b) Detailed chemical composition of the CoO_xN_y thin films as a function of $y/(x+y)$.

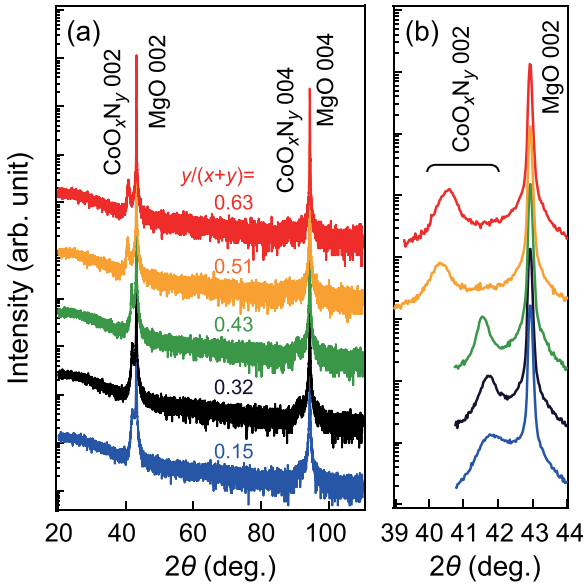

FIG. 3. θ–2θ XRD patterns of CoO_xN_y thin films grown on MgO (100) with various nitrogen contents. (a) Wide scans and (b) magnified plots near the 002 diffraction peaks.

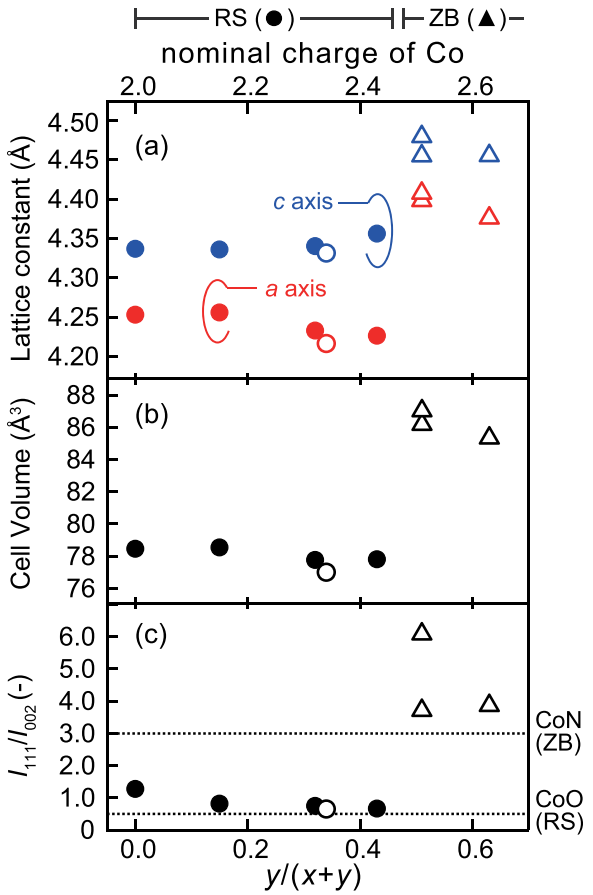

FIG. 4. Lattice parameters of CoO_xN_y thin films grown on MgO (100) with various nitrogen contents; (a) in-plane (*a* axis) and out-of-plane (*c* axis) lattice constants calculated from the 002 and 111 diffraction peaks, (b) unit cell volumes, and (c) intensity ratios of the 111 to 002 diffraction peaks. The circles and triangles indicate the RS and ZB structures, respectively. The filled symbols indicate the films fabricated under $P_{N_2} = 1 \times 10^{-5}$ Torr, and the open ones indicate the films fabricated under $P_{N_2} = 4 \times 10^{-5}$ Torr. The dotted lines in (c) indicate the reported values for CoO (RS structure) and CoN (ZB structure).

diffraction I_{111}/I_{002} is a good way to distinguish RS and ZB structures:[25] I_{111}/I_{002} is ~0.5 for RS CoO[26] and ~3 for ZB CoN.[25] Figure 4 summarizes the in-plane (*a* axis) and out-of-plane (*c* axis) lattice constants, unit cell volumes, and I_{111}/I_{002} values of the CoO_xN_y thin films. The I_{111}/I_{002} values and in-plane lattice constants were evaluated from 002 and 111 diffraction of the same film grown on MgO (100) substrate. All these structural parameters abruptly increased at $y/(x+y) \sim 0.5$. The I_{111}/I_{002} values at $y/(x+y) \leq 0.43$ and $y/(x+y) \geq 0.51$—0.6–1.2 and 3.7–6.1, respectively—are consistent with those expected for RS and ZB. Furthermore, the increase in unit cell volume at $y/(x+y) = \sim 0.5$, ~10%, is equivalent to that predicted by the first-principles calculation of CoN with RS and ZB structures, ~25%.[27] These results indicate that the structural phase transition from RS to ZB occurred at $y/(x+y) \sim 0.5$. We note that all of the films showed tetragonal distortion ($c > a$) due to compressive strain from the substrate. While the lattice constants slightly depended on film thickness due to partial relaxation from the substrate ($a > a_{MgO}$), the influence of film thickness on the lattice constant was small for the samples thicker than 50 nm (see supplementary Fig. S2[24]).

The structural phase transition at $y/(x+y) \sim 0.5$ might have been caused by a change in the average electronegativity of the anions. According to the Mooser–Pearson plot,[28] the coordination numbers of materials tend to decrease with a decrease of average principal quantum number *n* or electronegativity difference between cations and anions, $\Delta\chi$. For CoO_xN_y, while $n = 3$ is constant, $\Delta\chi$ decreases from ~1.8 (CoO) to ~1.3 (CoN)[29] as the nitrogen content *y* increases from 0 to 1, which would induce the phase transition from RS (6 coordination) to ZB (4 coordination).

We also studied the electrical transport properties of the RS- and ZB-CoO_xN_y thin films with various anion compositions. Figure 5(a) shows the electrical resistivity ρ of the CoO_xN_y thin films at room temperature. With increasing nitrogen content, the ρ of the RS-CoO_xN_y thin films ($y/(x+y) \leq 0.43$) monotonically decreased from the order of $10^5\,\Omega$ cm to $10^{-3}\,\Omega$ cm. This tendency is rationalized by considering hole doping into *p*-type CoO through nitrogen substation for oxygen, although the high resistivity of the samples prevented verification of carrier type by Hall measurement. Notably, ρ abruptly decreased between $y/(x+y) = 0.32$ and 0.34. At the same time, the ρ–T curves of these films (inset of Fig. 5(a)) changed drastically: the insulating $d\rho/dT$ (on the order of $d(\rho/\rho_{300\,K})/dT \sim 10^{-2}\,K^{-1}$) at $y/(x+y) = 0.32$ changed to $d(\rho/\rho_{300\,K})/dT \sim 0$ at $y/(x+y) = 0.34$. The $d\rho/dT$ value finally became positive (i.e., metallic) at $y/(x+y) = 0.43$ ($T > 50$ K). These changes strongly suggest that CoO_xN_y underwent an insulator-to-metal transition (IMT) at $y/(x+y) = \sim 0.34$. We stress that a low ρ on the $10^{-3}\,\Omega$ cm order together with composition-induced IMT has not yet been reported in Co^{2+}/Co^{3+} mixed valence cobalt oxides with octahedral coordination such as Co_3O_4,[17] Li-doped CoO ($Li_xCo_{1-x}O$),[15,16] or $La_{1-x}Sr_{1+x}CoO_4$.[18]

The ρ values of the ZB-CoO_xN_y ($y/(x+y) \geq 0.51$) films are on the same order as that of polycrystalline ZB-$CoO_{0.5}N_{0.5}$ thin film containing an amorphous impurity phase, $\rho \sim 10^{-3}\,\Omega$ cm,[14] confirming that such a low ρ is

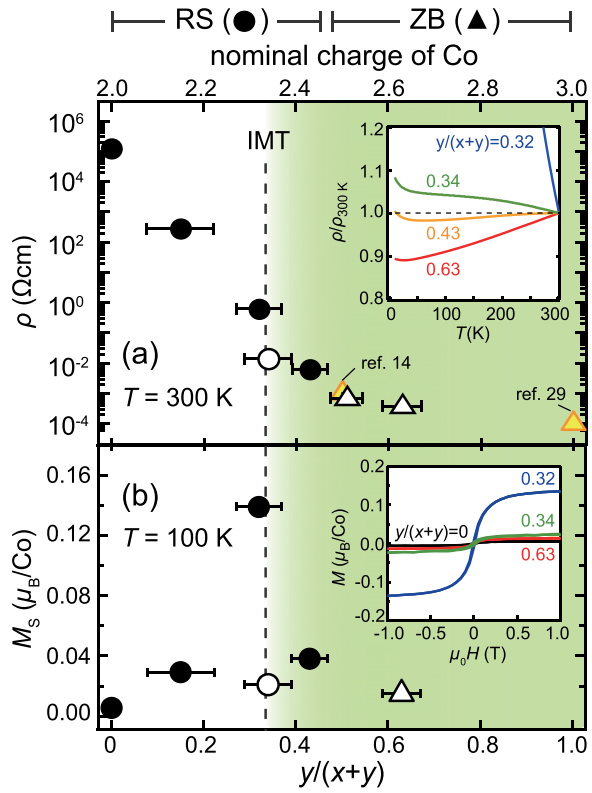

FIG. 5. (a) Resistivity of the CoO_xN_y thin films with various nitrogen contents at 300 K. The inset shows the temperature dependence of resistivity for several CoO_xN_y thin films. The vertical dashed line shows the composition of the insulator-to-metal transition. (b) Saturation magnetization (M_S) of the CoO_xN_y thin films with various nitrogen contents at 100 K. The inset shows the *M–T* curves of several CoO_xN_y thin films. The magnetic field was applied perpendicular to the film surface. The circles and triangles indicate the RS and ZB structures, respectively. The filled symbols indicate the films fabricated under $P_{N_2} = 1 \times 10^{-5}$ Torr, and the open ones indicate the films fabricated under $P_{N_2} = 4 \times 10^{-5}$ Torr.

intrinsic to ZB-CoO_xN_y. At $y/(x+y) = 0.63$, $\rho_{300\,K}$ reached $3.6 \times 10^{-4}\,\Omega$ cm, which is comparable with that of CoN ($1 \times 10^{-4}\,\Omega$ cm (Ref. 30)). The *ρ–T* curves of the ZB-CoO_xN_y films exhibited metallic temperature dependence ($d\rho/dT > 0$), as shown in the inset of Fig. 5(a).

Next, we discuss the spin state of the RS-CoO_xN_y phase. For Co^{2+}/Co^{3+} mixed valence systems with octahedral coordination, their electrical transport strongly depends on the spin state of Co^{3+}. While Co^{2+} is usually in the high-spin (HS) state, Co^{3+} can take the HS, intermediate spin (IS), or low-spin (LS) state depending on the crystal field.[31] Among these possible Co^{3+} spin states, we exclude LS Co^{3+} because electron transfer between HS Co^{2+} ($t_{2g}^5e_g^2$, $S = 3/2$) and LS Co^{3+} ($t_{2g}^6e_g^0$, $S = 0$) is blocked as a result of the large difference in spin angular momentum *S*.[31,32] We speculate that the Co^{3+} ions in the RS-CoO_xN_y exist in the IS state for the following reasons: (1) the low ρ is more likely explained by electron transfer between HS Co^{2+} and IS Co^{3+} ($t_{2g}^5e_g^1$, $S = 1$) through e_g orbitals, which overlap more strongly with the 2*p* orbitals of the anions, than by electron transfer between HS Co^{2+} and HS Co^{3+} ($t_{2g}^4e_g^2$, $S = 2$) through t_{2g} orbitals;[33] and (2) the lowered crystal field symmetry of the $CoO_{6-n}N_n$ octahedra ($n = 1, 2, \ldots 5$) stabilizes the IS state by removing the degeneracy of two e_g orbitals.

Finally, we briefly discuss the magnetic properties of the CoO_xN_y thin films. Figure 5(b) summarizes the *M–H* curves and saturation magnetization (M_S) of the CoO_xN_y films at 100 K. Because CoO is an antiferromagnetic Mott insulator, hole doping through nitrogen substitution would affect its magnetic properties. Indeed, the M_s of the RS-CoO_xN_y films increased as the nitrogen content $y/(x+y)$ increased from 0 to 0.32. The small hysteresis ($H_C \sim 100$ Oe) in the *M–H* curves may suggest weak ferromagnetism in these films. This systematic increase in M_S values ($\leq \sim 0.14\,\mu$B/Co) might be attributable to an increase in spin-canting angle induced by introduction of Co^{3+}, although the detailed mechanism remains unclear. However, further increasing the nitrogen content ($y/(x+y) \geq 0.34$) caused M_s to drop suddenly. We speculate that a magnetic phase transition occurred during the IMT of RS-CoO_xN_y. An interesting feature is that the phase transition occurred at $y/(x+y) \approx 1/3$, corresponding to local coordination geometry in which two of six anion sites of CoX_6 octahedra are occupied by nitrogen. This suggests that the phase transition was caused by a special coordination structure, such that apical oxygen were fully substituted with nitrogen. Unfortunately, it was difficult to determine whether the metallic RS-CoO_xN_y and ZB-CoO_xN_y phases were paramagnetic or antiferromagnetic because precise interpretations of the *M–T* curves were strongly hindered by the magnetic impurities in the MgO substrate.[34] Spectroscopic techniques such as X-ray absorption near edge structure and X-ray magnetic circular dichroism might give further information on the coordination structure, magnetic properties, and spin state of CoO_xN_y.

In summary, we synthesized CoO_xN_y epitaxial thin films ($0 \leq y/(x+y) \leq 0.63$) on MgO (100) single-crystalline substrates by using NPA-PLD. The obtained CoO_xN_y thin films showed a structural phase transition from RS to ZB as $y/(x+y)$ increased to ~0.5. The room-temperature electrical resistivity of the CoO_xN_y films varied widely from $10^5\,\Omega$ cm to $10^{-4}\,\Omega$ cm with nitrogen content. Notably, IMT appeared at $y/(x+y) \sim 0.34$ in the RS-CoO_xN_y phase, whereas the RS-CoO_xN_y phase with higher nitrogen content showed a low resistivity in the order of $1 \times 10^{-3}\,\Omega$ cm, possibly caused by the high electron-transfer rate between HS Co^{2+} and IS Co^{3+}. An abrupt decrease in saturation magnetization suggests that a magnetic phase transition occurred simultaneously with the IMT, though further investigation is needed to understand the detailed magnetic properties of CoO_xN_y. These results demonstrate that low-temperature epitaxial growth is a promising synthesis route for mid- to late-transition metal oxynitrides, which paves the way for exploring novel electronic functionalities in oxynitrides.

We thank Professor Hiroyuki Matsuzaki of The University of Tokyo for his assistance in ERDA measurements. We also appreciate Mr. Masahito Sano and Mr. Tomoya Onozuka, Mr. Naoki Kashiwa, and Mr. Shunsuke Shibata of The University of Tokyo for their assistance in evaluating the magnetic properties and a part of XRD measurements, respectively. This study was supported by the Ministry of Education, Culture, Sports, Science, and Technology (MEXT), Japan (KAKENHI No. 24760005). A part of this work was supported by the

"Nanotechnology Platform" (Project No. 12024046) of MEXT, Japan.

[1]M. Jansen and H. P. Letschert, Nature **404**, 980 (2000).
[2]E. Guenther and M. Jansen, Mater. Res. Bull. **36**, 1399 (2001).
[3]A. Fuertes, Dalton Trans. **39**, 5942 (2010).
[4]A. Kasahara, K. Nukumizu, G. Hitoki, T. Takata, J. N. Kondo, M. Hara, H. Kobayashi, and K. Domen, J. Phys. Chem. A **106**, 6750 (2002).
[5]A. Kasahara, K. Nukumizu, T. Takata, J. N. Kondo, M. Hara, H. Kobayashi, and K. Domen, J. Phys. Chem. B **107**, 791 (2003).
[6]K. Maeda, K. Teramura, D. Lu, T. Takata, N. Saito, Y. Inoue, and K. Domen, Nature **440**, 295 (2006).
[7]M. Yang, J. Oró-Solé, A. Kusmartseva, A. Fuertes, and J. P. Attfield, J. Am. Chem. Soc. **132**, 4822 (2010).
[8]D. Logvinovich, J. Hejtmánek, K. Knížek, M. Maryško, N. Homazava, P. Tomeš, R. Aguiar, S. G. Ebbinghaus, A. Reller, and A. Weidenkaff, J. Appl. Phys. **105**, 023522 (2009).
[9]S. G. Ebbinghaus, H. P. Abicht, R. Dronskowski, T. Müller, A. Reller, and A. Weidenkaff, Prog. Solid State Chem. **37**, 173 (2009).
[10]O. Diwald, T. L. Thompson, T. Zubkov, E. G. Goralski, S. D. Walck, and J. T. Yates, J. Phys. Chem. B **108**, 6004 (2004).
[11]A. Kafizas, G. Hyett, and I. P. Parkin, J. Mater. Chem. **19**, 1399 (2009).
[12]P. Tomeš, D. Logvinovich, J. Hejtmánek, M. H. Aguirre, and A. Weidenkaff, Acta Mater. **59**, 1134 (2011).
[13]F. C. Voogt, P. J. M. Smulders, G. H. Wijnja, L. Niesen, T. Fujii, M. A. James, and T. Hibma, Phys. Rev. B **63**, 125409 (2001).
[14]N. R. M. Crawford, J. S. Knutsen, K. A. Yang, G. Haugstad, S. McKernan, F. B. McCormick, and W. L. Gladfelter, Chem. Vap. Deposition **4**(5), 181 (1998).
[15]T. Sato, C. H. Chang, T. Endo, and M. Shimada, J. Mater. Sci. Lett. **5**, 552 (1986).
[16]A. J. Bosman and C. Crevecoeur, J. Phys. Chem. Solids **30**, 1151 (1969).
[17]C. S. Cheng, M. Serizawa, H. Sakata, and T. Hirayama, Mater. Chem. Phys. **53**, 225 (1998).
[18]Y. Moritomo, K. Higashi, K. Matsuda, and A. Nakamura, Phys. Rev. B **55**, R14725 (1997).
[19]S. Sasaki, K. Fujino, and Y. Takeuchi, Proc. Jpn. Acad., Ser. B **55**, 43 (1979).
[20]T. B. Joyner and F. H. Verhoek, J. Am. Chem. Soc. **83**, 1069 (1961).
[21]D. Oka, Y. Hirose, T. Fukumura, and T. Hasegawa, Cryst. Growth Des. **14**, 87 (2014).
[22]A. Suzuki, Y. Hirose, D. Oka, S. Nakao, T. Fukumura, S. Ishii, K. Sasa, H. Matsuzaki, and T. Hasegawa, Chem. Mater. **26**, 976 (2014).
[23]D. Oka, Y. Hirose, H. Kamisaka, T. Fukumura, K. Sasa, S. Ishii, H. Matsuzaki, Y. Sato, Y. Ikuhara, and T. Hasegawa, Sci. Rep. **4**, 4987 (2014).
[24]See supplementary material at http://dx.doi.org/10.1063/1.4937431: In supplementary Fig. S1 we show phi scan plots of the CoO_xN_y thin films. In Fig. S2 we indicate thickness dependence of the lattice constants of the CoO_xN_y thin film.
[25]K. Suzuki, T. Kaneko, H. Yoshida, H. Morita, and H. Fujimori, J. Alloys Compd. **224**, 232 (1995).
[26]R. K. Gupta, A. K. Sinha, B. N. R. Sekhar, A. K. Srivastava, G. Singh, and S. K. Deb, Appl. Phys. A **103**, 13 (2011).
[27]P. Lukashev and W. R. L. Lambrecht, Phys. Rev. B **70**, 245205 (2004).
[28]E. Mooser and W. B. Pearson, Acta Crystallogr. **12**, 1015 (1959).
[29]W. Gordy and W. J. O. Thomas, J. Chem. Phys. **24**, 439 (1956).
[30]L. Maya, M. Paranthaman, J. R. Thompson, T. Thundat, and R. J. Stevenson, J. Appl. Phys. **79**, 7905 (1996).
[31]B. Raveau and M. M. Seikh, *Cobalt Oxides: From Crystal Chemistry to Physics* (Wiley-VCH, 2012).
[32]A. Maignan, V. Caignaert, B. Raveau, D. Khomskii, and G. Sawatzky, Phys. Rev. Lett. **93**, 026401 (2004).
[33]M. Imada, A. Fujimori, and Y. Tokura, Rev. Mod. Phys. **70**, 1039 (1998).
[34]J. Orna, P. A. Algarabel, L. Morellón, J. A. Pardo, J. M. de Teresa, R. L. Antón, F. Bartolomé, L. M. García, J. Bartolomé, J. C. Cezar, and A. Wildes, Phys. Rev. B **81**, 144420 (2010).